

# Effects of Intermolecular Interaction and Molecule–Electrode Couplings on Molecular Electronic Conductance

Hua Geng, Shiwei Yin, Ke-Qiu Chen, and Zhigang Shuai\*

Laboratory of Organic Solids, Center for Molecular Science, Institute of Chemistry, Chinese Academy of Sciences, 100080 Beijing, PRC

Received: February 5, 2005; In Final Form: April 4, 2005

By applying nonequilibrium Green's function and first-principle calculation, we investigate the transport behavior of a prototype of a molecular device. The intermolecular interaction and molecule–electrode coupling effects are analyzed in detail, through which we can gain insight into the complexities within a molecular device such as intermolecular charge transport contributions and the imperfect molecule–electrode contact. The existing discrepancy between theory and experiment is discussed.

## I. Introduction

In recent years, progress in microfabrication and self-assembly techniques<sup>1</sup> has made it possible to design a single-molecule device. The electronic transport properties of single-molecule junctions or molecular devices have attracted much attention because of their novel physical properties and potential for device application, including single-electron characteristics,<sup>2</sup> negative differential resistance,<sup>3</sup> electrostatic current switching,<sup>4–6</sup> etc. Various kinds of single-molecule junctions or molecular–monolayer junctions, such as atomic wires,<sup>7</sup> short organic molecule wires,<sup>8–10</sup> long-chain polymers,<sup>11</sup> carbon nanotubes,<sup>12</sup> and fullerenes,<sup>13</sup> have been reported.

1,4-Dithiolbenzene (DTB) is one of the systems most intensely studied as a prototype of molecular transport theory<sup>14–24</sup> since the self-assembled monolayer (SAM) measurement for the device with DTB was reported.<sup>8</sup> However, the calculated  $I$ – $V$  characteristics were more than 2 orders of magnitude larger than the experimental results of Reed et al.<sup>8</sup> It is suggested that the most plausible origin of the discrepancy between calculations and the experiment lies in the contact. At present, it is difficult to manipulate the contact between molecule and electrode and investigate its influence on the electron transport experimentally. To understand the observed experimental results, the effects of various geometry contacts on electron transport were studied. Emberly and Kirczenow<sup>25</sup> considered a junction between two DTB molecules with perpendicular phenyl rings, and found that such an arrangement will strongly reduce the conductance. Stockbro and co-workers<sup>26</sup> calculated the  $I$ – $V$  characteristics of DTB coupled to two Au(111) surfaces via either thiol or thiolate bonds. They found that the  $I$ – $V$  spectrum and conductance are qualitatively different for the different bonds between molecule and Au(111) surfaces. However, the calculated differential conductance is several orders of magnitude higher than the experimental values. Xue and Ratner<sup>27</sup> have also investigated the effect on molecular transport due to the different structural aspects of metal–molecule interfaces. Their results show that the presence of the additional hydrogen end atom at the top metal–molecule contact substantially affects the electronic processes in the molecular junction and reduces conductance

and current. Recently, Liu et al.<sup>28</sup> investigated the effects of lateral interactions on the conductance of two benzene molecules connected in parallel to semi-infinite leads. They found that intermolecular interaction occurs indirectly through the Au electrodes and leads to an increase in conductance. A recent work by Delaney and Greer ascribes the discrepancy to the electron correlation effects in molecules.<sup>29</sup>

In this work, we consider a possible configuration for the SAM: two cofacial benzenes sandwiched between semi-infinite gold electrodes. One contact between one molecule and the electrode is a strong chemical bond through the thiol end group, while a certain distance exists between the electrode and the other end of the molecule, where the strong S–H bond has not been cleaved. For the second molecule, the contact situation is just reversed, as shown in Figure 1. We believe that in the molecular self-assembly monolayer, the transport behavior depends on the intermolecular interaction as well as the molecule–electrode contact. In this work, we present a detailed theoretical study on the device structure shown in Figure 1, which consists of (i) the intermolecular charge transport channel and (ii) the imperfect molecule–electrode contact, where both the intermolecular distance and the interelectrode distance are varied, and we make a detailed analysis between this configuration with the perfect one-molecule device. Under the experimental conditions, the perfect contact is not guaranteed at this stage; thus, the device configuration we proposed exists in the real situation. In fact, the measured conductance for a single molecule is derived from the total conductance divided by the number of molecules in the SAM, under the following assumptions. (i) There is no intermolecular transport channel, and the quantum interference between different channels is neglected: in fact, for the case of packed conjugated molecules,<sup>30–32</sup> the interaction through the delocalized  $\pi$ -orbital could strongly mask the individual contribution from the presumably isolated molecule. (ii) The case in which one molecule is bonded with one electrode is much easier to be realized in experiment than with both electrodes; namely, the electron transport from one end can be very efficient, but when one moves to another end, the electron would either tunnel to another electrode or jump to a neighboring molecule, which is probably connected to another electrode. In such situations, the  $I$ – $V$  curve is still symmetric as demonstrated in the experiments

\* To whom correspondence should be addressed. E-mail: zgshuai@iccas.ac.cn.

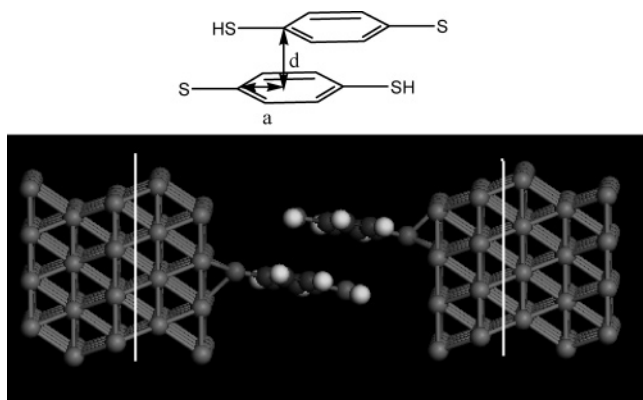


**Figure 1.** Configuration of the device in our simulation. The periodical boundary conditions are applied in the  $x$  and  $y$  directions, and the electrode extends along the  $z$  axis to infinity. Atoms in the region within the two white lines are included in the self-consistent cycle, including two layers of  $4 \times 4$  Au atoms from the (111) surface, while the remainder of the electrodes are described by employing bulk Hamiltonian parameters and self-energy (energy shifted according to the applied bias) on gold atoms in the third and fourth layers.

of Reed et al.,<sup>8</sup> but the conductance is expected to be much smaller than the single molecule with the perfect contact. By applying the first-principles methods to simulate different intermolecular distances and different interelectrode separation, we can gain a deeper understanding of the transport behavior in the real situation in the molecular electronic device.

In this paper, the first-principles electron transport theory is applied to calculate the transmission coefficient and the current–voltage curves. Recently, there have been several first-principles theoretical studies of electron transport in organic molecules under finite bias conditions,<sup>18,20,21,33–36</sup> which differs mainly in their description of semi-infinite electrodes and their interaction with the molecules in the contact region. The method we use here is a first-principles nonequilibrium Green’s function-based electronic transport package, Transiesta-c, developed by Brandbyge and co-workers.<sup>36</sup> The method is based on density functional theory and can treat the molecule–electrode system self-consistently under finite bias conditions.

We first investigated the transmission coefficient, the projected density of the state, and the molecular electronic state within the environment of the electrode under zero bias and then illustrated the current–voltage behaviors, and their dependence on the intermolecular and interelectrode distances. We highlight the importance of intermolecular electron transport.

## II. Computational Procedure

The first-principles nonequilibrium Green’s function method has been described in detail in ref 36. Here we will present only the technical details specific to our calculations. Figure 1 shows the device setup for simulation: two DTB molecules spanning the gap between the electrodes. The Au electrode is cleaved on the (111) surface. The end group of the molecule contacting the electrode is positioned in the FCC site of the Au surface, as shown by Gronbeck et al.,<sup>37</sup> while the S–H bond has not been cleaved for the other (nonbonding) end. The distance from this end group to the electrode depends on the electrode–electrode separation. The distance between the molecular planes of the two DTBs ( $d$ ) has been first chosen to be 3.6 Å, a typical value for phenyl ring stacking. The electronic structure is calculated via self-consistent DFT with local density approximation. Core electrons are modeled with Troullier–Martins<sup>38</sup> nonlocal pseudopotentials, while the valence electrons

are expanded in a SIESTA localized basis set. We use the double  $\zeta$  + polarization basis set for the organic molecule, and a single  $\zeta$  for the Au atom.

We use periodic boundary conditions for the DFT calculation in the contact region, a supercell consisting of two layers of  $4 \times 4$  Au and the two molecules. It is reported that taking two layers of gold in the self-consistent cycle is enough to avoid the finite size effect.<sup>6,26,36</sup> Furthermore, in the literature, a  $3 \times 3$  supercell has been used.<sup>6,26</sup> Our  $4 \times 4$  supercell is large enough to avoid any interaction with molecules in the next supercell. As a result, there is no effect of the surface on the geometry of the contact region, while the remainders of electrodes are described by bulk parameters. These are determined from separate calculations for the bulk phase of gold employing the same model. Using a Green’s function technique, the electronic structure of the semi-infinite electrode can be projected into the third and fourth Au layers.

In this approach, the molecular vibration effects have been neglected. As we know, in bulk materials the transport behavior is dominated by the carrier scattering with phonons, while in a meso-scale system the ballistic transport becomes important. The molecular electronic system is on the order of nanometers, falling in the ballistic transport range. We have fixed the molecular geometry; in other words, we have assumed that the electron transport through the device is so quick that there is no time for the molecules to deform. This is also generally assumed in many other investigations.<sup>6,16,19,21–23</sup> The molecular vibration effects under bias have been discussed by Alavi et al.<sup>39</sup> in the single-molecule configuration.

## III. Results and Discussion

In panels a and b of Figure 2, we show the projected partial density of states (PDOS), namely, the density of states of the combined system projected onto all the molecule subspace, and the transmission coefficient  $T(E, V_b)$  for the bimolecular systems (shown in Figure 1) as a function of electron energy at zero bias ( $V_b = 0$ ). As a comparison, in Figure 2c, we give the transmission coefficient of the single-DTB molecule configuration for the same electrode–electrode distance. Here, the distance between left and right electrodes is 10.65 Å, corresponding to a horizontal intermolecular distance ( $a$ ) of 0.5 Å. The energy origin is set to be the Fermi level of the system. From panels a and b of Figure 2, it is clearly seen that the  $T(E)$  and the PDOS are strongly correlated, especially in the location of their peaks. The transmission curve consists of a series of peaks, and shows the same qualitative features as the projected PDOS. It is known that the PDOS represents the discrete energy levels of the isolated molecule, which include the effects of energy shift and line broadening due to the molecule–electrode coupling. The transmission is determined by the electronic structure of the molecule and the coupling: the peak corresponds to the resonant transmission through the molecular states. When comparing panels b and c of Figure 2, we find that more transmission peaks appear in the bimolecular systems, which means that more transmission channels are open in this system than in single-molecule systems. Moreover, peak values and their positions are different in single-molecule and bimolecular systems. All these indicate that the intermolecular interaction may play an important role in electronic transport for the bimolecular system presented here. The intermolecular coupling may involve two types of interactions: direct molecule–molecule interaction between benzene molecules and indirect interaction through the gold surfaces. From ref 28, it is known that for the system with two parallel molecules in a plane, the

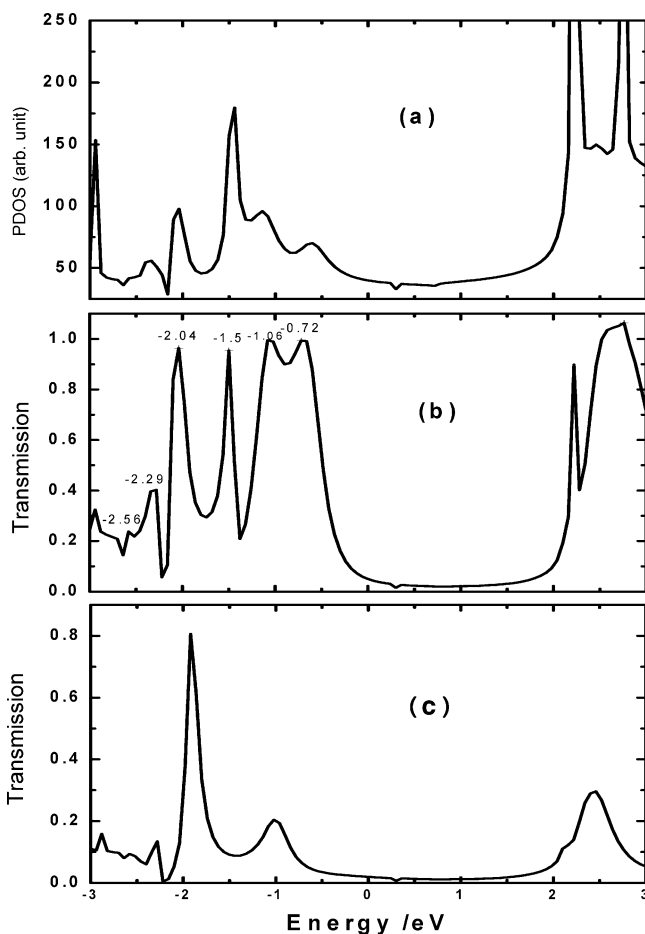


**Figure 2.** PDOS (a) and the transmission coefficients (b) for the DTB bimolecular device. For comparison, the transmission coefficient for the single DTB with one end coupled to Au(111) electrodes with the same electrode separation of 10.65 Å is depicted (c).

dominant interaction between the molecules is an indirect one through the Au electrodes. However, for the system with two carbon chains connected in parallel between two flat metal electrodes, both direct and indirect interactions are responsible for the conductance.<sup>7</sup> It is thus intriguing to investigate the evolution from a single molecule to the present bimolecular systems, shown in Figure 1, which is different from either ref 28 in which only one end of both molecules is covalently connected to one side of the metal surface or ref 7 in which both ends of the pair of atomic wires are connected to both sides of the metal surface.

To understand the origins of the peaks in transmission curves, we analyze the molecularly projected self-consistent Hamiltonian (MPSH), which is the molecular part extracted from the whole self-consistent Hamiltonian for the contact region (two layers of Au electrode in the left with the molecule and another two Au layers on the right-hand side; see ref 26). Thus, it contains the molecule–electrode coupling effects because during the self-consistent iteration, the electron density is for the contact region as a whole.

Panels a<sub>1</sub>–a<sub>3</sub> of Figure 3 show three frontier molecular orbitals of the MPSH for the single-molecule system, while panels b<sub>1</sub>–b<sub>6</sub> of Figure 3 show six frontier molecular orbitals of the MPSH for the bimolecular system. The MPSH does not include the self-energy of the electrodes. The imaginary part of the self-energy broadens the transmission peaks, while the real part gives a rigid shift of the peak relative to the MPSH states. In general, the stronger the coupling between the molecule and

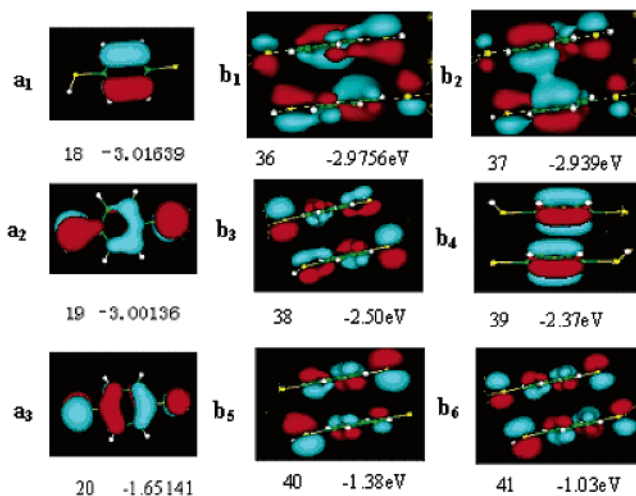


**Figure 3.** Frontier orbitals of the MPSH. Plots a<sub>1</sub>–a<sub>3</sub> are the HOMO-2, HOMO-1, and HOMO, respectively, for a single DTB molecule in the device. Plots b<sub>5</sub> and b<sub>6</sub> are the two splitting components of the HOMO, plots b<sub>1</sub> and b<sub>3</sub> the splittings of the HOMO-1, and plots b<sub>2</sub> and b<sub>4</sub> the splittings of the HOMO-2. These can be readily seen from the shapes of the corresponding orbitals.

the electrode, the broader the corresponding transmission peak. In fact, the density distributions of the orbitals can reveal information about the coupling between the molecule and the solid surface as well as between molecules in a picturesque way. For a cofacially separated conjugated molecule pair, the frontier molecular orbitals will split. The magnitude of the splitting is dependent on the relative position of the interacting molecules.<sup>40</sup> With respect to the bimolecular system presented here, orbitals 40 (panel b<sub>5</sub>) and 41 (panel b<sub>6</sub>) originate from the two splitting components from the HOMO (Figure a<sub>3</sub>) of the original DTB molecule, which is readily seen from their orbital distributions. These two MPSH orbitals have a high density on the sulfur atom, which means much stronger molecule–electrode interaction. These correspond to the two broad peaks, centered at  $-0.72$  and  $-1.06$  eV (splitting = 0.34 eV), respectively, in the transmission curve. Similarly, we find that orbitals 37 (panel b<sub>1</sub>) and 39 (panel b<sub>4</sub>) originate from the HOMO-2 of the single DTB molecule, both having a vanishingly small effect on the coupling of the sulfur atom to the electrode. It explains the two narrow peaks centered at  $-1.5$  and  $-2.29$  eV (splitting = 0.79 eV), due to the weak molecule–electrode interaction. Very similar situations occur for orbitals 36 (panel b<sub>2</sub>) and 38 (panel b<sub>3</sub>), splitting from the HOMO-1 of the single molecule. These orbitals present large density weights at sulfur, with resulting broad transmission peaks at approximately  $-2.04$  and  $-2.56$  eV (splitting = 0.42 eV). It is noted that the sizes of the splitting vary from orbital to orbital. In fact, the splitting is determined by both the intermolecular coupling and the molecule–electrode interaction: the orbital energies are the MPSH states. From the point of view of intermolecular coupling, the splitting is proportional to the overlap of the interacting orbitals. From Figure 3, it is seen that the HOMO-2 (orbitals 37 and 39) presents a large electron cloud in the interacting (cofacially overlapping) regions; thus, it presents a large orbital spitting. Thus, the MPSH analysis has revealed that the intermolecular interaction effect is remarkable on the electronic structures as well as the transmission peaks. We note that the quasi-probability density analysis in the literature can also take into account the self-energy contribution, which might be more advantageous as it contains the openness of the system.<sup>41</sup>

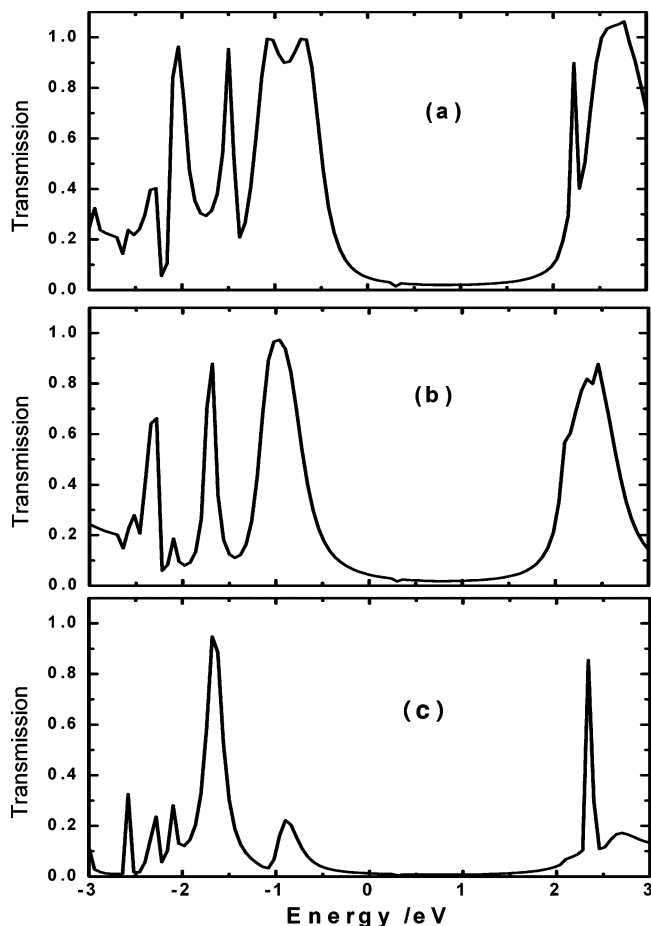


**Figure 4.** Dependence of the transmission coefficients on the electrode separation for (a) 10.65, (b) 11.15, and (c) 11.63 Å, corresponding to horizontal intermolecular distances (*a*) of 0.5, 1.0, and 1.5 Å, respectively.

For the bimolecular system, there are two possible electron transport pathways: (a) electron moving directly from the left electrode directly to the DTB molecule and then tunneling to the right electrode and (b) electron moving from the left electrode to one molecule and then hopping to another molecule, which is covalently bonded with the right electrode, and finally to the electrode. Lang and Avouris have shown that the conductance for a pair of atomic wires is strongly dependent on the wire separation.<sup>7</sup> They found that both direct and indirect interwire interactions are important. Indeed, as pointed out by Liu et al., the indirect intermolecular interaction via the electrode where both molecules are attached comes into play in increasing the conductance.<sup>28</sup> In our case, the indirect intermolecular interaction is negligible, because the two molecules in question are covalently linked to different electrodes. Here, all the intermolecular effects come from direct interaction.

In Figure 4, we illustrate the effect of the distance between two electrodes on transmission coefficient  $T(E, V_b)$  for the bimolecular system at zero bias ( $V_b = 0$ ). With an increase in the electrode separation, the extent of primary tunneling from the molecule to the electrode (first pathway) is reduced drastically, which results from the increase in the barrier between the S–H end of the molecule and the metal surface. However, for the second pathway, the reduction is mainly due to decreasing intermolecular overlap. It is interesting to note that the two broad transmission peaks, at  $-0.72$  and  $-1.06$  eV, merge gradually, and become one small peak eventually. This can be understood from the interaction of molecular orbitals.

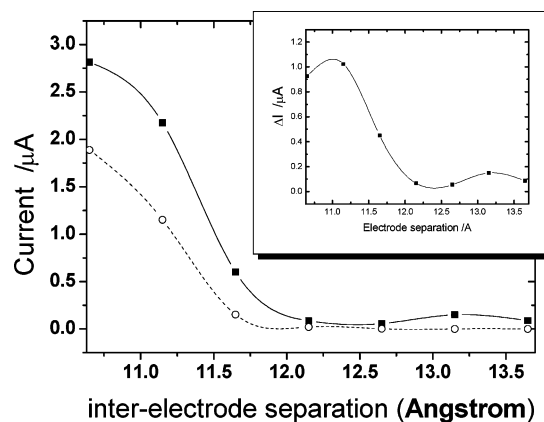


**Figure 5.** Comparison of bimolecule and monomolecule device currents, as a function of electrode separation. The bias is fixed at 0.6 V. The vertical distance of the molecular plane for the bimolecule system is 3.6 Å. The current value for the monomolecule device is obtained as described in ref 43, namely, the sum of two monomolecule devices. The solid line is for the bimolecule device, and the dotted line is for the sum of two monomolecule devices. The inset shows their difference.

When the distance between two electrodes is increased, the size of the intermolecular overlapping region is reduced, and then the HOMO splitting becomes smaller. At the same time, the likelihood of intermolecular hopping between the two DTB molecules is reduced. We will further discuss this behavior in more detail in the following  $I$ – $V$  curve section.

We now turn to investigating current–voltage ( $I$ – $V$ ) characteristics for different distances between the two electrodes. For each bias, the electronic structure is determined self-consistently under the nonequilibrium conditions. The current is calculated by the Landauer–Büttiker formula:<sup>42</sup>  $I = \int_{\mu_L}^{\mu_R} T(E, V_b) dE$ , where  $\mu_L$  and  $\mu_R = \pm eV_b$  and  $T(E, V_b)$  is the transmission probability for electrons incident at an energy  $E$  through a device under a bias  $V_b$ . Since the device structure is symmetric, the  $I$ – $V$  curve is also symmetric with respect to the bias polarity.

To reveal the effects of intermolecular interaction on transport, we first compared the current dependence on the electrode separations for the monomolecule and bimolecule situation; see Figure 5. For a fixed electrode separation, we can define the relationship  $\Delta I = I_b - I_m$ , where  $I_b$  and  $I_m$  are the current of the bimolecule and monomolecule devices, respectively. This represents the pure current flow through the intermolecular pathway (b), shown in the insert of Figure 5. We note that with the increase in the electrode separation, the magnitude of the current from the single-molecule pathway (a) is decreased remarkably. The inset of Figure 5 clearly depicts the intermolecular current for pathway b. In Figure 6, we depict the ratio of the current through intermolecular transport to the total current as a function of electrode separation. It is evident that with the increase in electrode separation, the percentage of the intermolecular pathway increases rapidly from 30 to 100%. The intermolecular interactions have induced orbit splitting. These additional orbits offer electron transport channels. We can see that the splitting of HOMO introduces a transmission peak close to Fermi energy in Figure 2b; according to the Landauer–Büttiker formula, when this transmission peak enters into the bias window, it would contribute to the total current.

Finally, we display the  $I$ – $V$  curves for different electrode separations in Figure 7. It is worth noting in particular that the features and the magnitude of the current–voltage ( $I$ – $V$ ) curves for electrode separation at 12.11 Å are in agreement with the

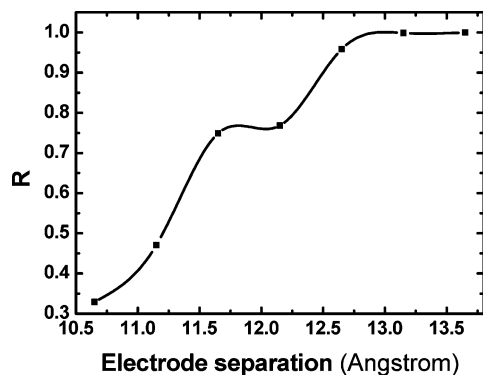


**Figure 6.** Ratio of intermolecular current contribution with respect to the total current, as a function of electrode separation.

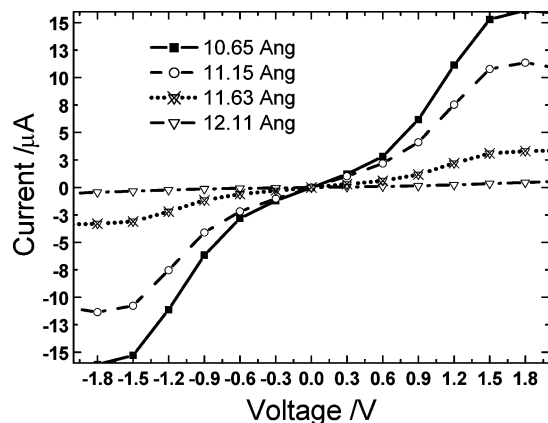


**Figure 7.**  $I$ – $V$  curves of the bimolecular device for different electrode separations.

experimental results. For instance, when  $V_b = 2$  V, the experimental current value is  $\sim 0.1 \mu\text{A}$ ,<sup>8</sup> while the calculated value is  $0.5 \mu\text{A}$ . We stress that the device configuration shown in this work is probably the real situation in the SAM structure.

#### IV. Conclusion

We have investigated from first-principles nonequilibrium Green's function the transmission properties of electrons in a cofacially separated two-molecule device system. The intermolecular interaction has been analyzed in detail. The transmission features have been assigned to the frontier orbital splittings. The result shows that the intermolecular interaction plays a critical role in determining the electron transmission. The calculated current–voltage ( $I$ – $V$ ) characteristics can be comparable to those of the experiment. These results will be helpful in understanding further the real situation in the molecular electronic device.

**Acknowledgment.** This work is supported by the National Science Foundation of China (Grants 90203015, 90301001, 90403026, and 10425420), the Ministry of Science and Technology of China, and the Supercomputing Center of the Chinese Academy of Sciences.

#### References and Notes

- (1) Andres, R. P.; Bein, T.; Dorogi, M.; Feng, S.; Henderson, J. I.; Kubiak, C. P.; Mahoney, W.; Osifchin, R. G.; Reifenberger, R. *Science* **1996**, *272*, 1323.
- (2) Chen, J.; Reed, M. A.; Rawlett, A. M.; Tour, J. M. *Science* **1999**, *286*, 1550.
- (3) Collier, C. P.; Wong, E. W.; Belohradsky, M.; Raymo, F. M.; Stoddart, J. F.; Kuekes, P. J.; Williams, R. S.; Heath, J. R. *Science* **1999**, *285*, 391.

- (4) Gittins, D. I.; Bethell, D.; Schiffrin, D. J.; Nichols, R. J. *Nature* **2000**, *408*, 67.
- (5) Donhauser, Z. J.; Mantooh, B. A.; Kelly, K. F.; Bumm, L. A.; Monnell, J. D.; Stapleton, J. J.; Price, D. W., Jr.; Rawlett, A. M.; Allara, D. L.; Tour, J. M.; Weiss, P. S. *Science* **2001**, *292*, 2303.
- (6) Stokbro, K.; Taylor, J.; Brandbyge, M. *J. Am. Chem. Soc.* **2003**, *125*, 3674.
- (7) Lang, N. D.; Avouris, P. *Phys. Rev. B* **2000**, *62*, 7325.
- (8) Reed, M. A.; Zhou, C.; Muller, C. J.; Burgin, T. P.; Tour, J. M. *Science* **1997**, *278*, 252.
- (9) Reichert, J.; Ochs, R.; Beckmann, D.; Weber, H. B.; Mayor, M.; Lohneysen, H. V. *Phys. Rev. Lett.* **2002**, *88*, 176804.
- (10) Xu, B.; Tao, N. J. *Science* **2003**, *301*, 121.
- (11) Hu, W.; Nakashima, H.; Furukawa, K.; Kashimura, Y.; Ajito, K.; Torimitsu, K. *Appl. Phys. Lett.* **2004**, *85*, 115.
- (12) Tans, S. J.; Verschueren, A. R. M.; Dekker, C. *Nature* **1999**, *393*, 49.
- (13) Yao, Z.; Postma, H. W. C.; Balents, L.; Dekker, C. *Nature* **1999**, *402*, 273.
- (14) Park, H.; Park, J.; Lim, A. K. L.; Anderson, E. H.; Alivisatos, A. P.; Mceuen, P. L. *Nature* **2000**, *407*, 57.
- (15) Emberly, E. G.; Kirczenow, G. *Phys. Rev. B* **1998**, *58*, 10911.
- (16) Olson, M.; Mao, Y.; Windus, T.; Kemp, M.; Ratner, M. A.; Leon, N.; Mujica, V. *J. Phys. Chem. B* **1998**, *102*, 941.
- (17) Yaliraki, S. N.; Roitberg, A. E.; Gonzalez, C.; Mujica, V.; Ratner, M. A. *J. Chem. Phys.* **1999**, *111*, 6997.
- (18) Hall, L. A.; Reimers, J. R.; Hush, N. S.; Silverbrook, K. *J. Chem. Phys.* **2000**, *112*, 1510.
- (19) Derosa, P. A.; Seminario, J. M. *J. Phys. Chem. B* **2001**, *105*, 471.
- (20) Xue, Y.; Datta, S.; Ratner, M. A. *J. Chem. Phys.* **2001**, *115*, 4292.
- (21) Damle, P. S.; Ghosh, A. W.; Datta, S. *Phys. Rev. B* **2001**, *64*, 201403.
- (22) Luo, Y.; Wang, C.-K.; Fu, Y. *J. Chem. Phys.* **2002**, *117*, 10283.
- (23) Di Ventra, M.; Pantelides, S. T.; Lang, N. D. *Phys. Rev. Lett.* **2002**, *88*, 46801.
- (24) Ke, S.-H.; Baranger, H. U.; Yang, W. *Phys. Rev. B* **2004**, *70*, 085410; *J. Am. Chem. Soc.* **2004**, *126*, 15897.
- (25) Karzazi, Y.; Crispin, X.; Kwon, O.; Brédas, J. L.; Cornil, J. *Chem. Phys. Lett.* **2004**, *387*, 502.
- (26) Emberly, E. G.; Kirczenow, G. *Phys. Rev. B* **2001**, *64*, 235412.
- (27) Stokbro, K.; Taylor, J.; Brandbyge, M.; Mozos, J.-L.; Ordejon, P. *Comput. Mater. Sci.* **2003**, *27*, 151.
- (28) Xue, Y.; Ratner, M. A. *Phys. Rev. B* **2003**, *68*, 115406; *Phys. Rev. B* **2003**, *68*, 115407.
- (29) Liu, R.; Ke, S.-H.; Baranger, H. U.; Yang, W. *J. Chem. Phys.* **2005**, *122*, 044703.
- (30) Delaney, P.; Greer, J. C. *Phys. Rev. Lett.* **2004**, *93*, 036805.
- (31) Cui, X. D.; Primak, A.; Zarate, X.; Tomfohr, J.; Sankey, O. F.; Moore, A. L.; Gust, D.; Harris, G.; Lindsay, S. M. *Science* **2001**, *294*, 571.
- (32) Cui, X. D.; Primak, A.; Zarate, X.; Tomfohr, J.; Sankey, O. F.; Moore, A. L.; Gust, D.; Harris, G.; Lindsay, S. M. *J. Phys. Chem. B* **2002**, *106*, 8609.
- (33) Kushmerick, J. G.; Naciri, J.; Yang, J. C.; Shashidhar, R. *Nano Lett.* **2003**, *3*, 897.
- (34) Taylor, J.; Guo, H.; Wang, J. *Phys. Rev. B* **2001**, *63*, 245407.
- (35) Wang, C.-K.; Fu, Y.; Luo, Y. *Phys. Chem. Chem. Phys.* **2001**, *3*, 5017.
- (36) Palacios, J. J.; Perez-Jimenez, A. J.; Louis, E.; Verges, J. A. *Phys. Rev. B* **2002**, *64*, 115411.
- (37) Brandbyge, M.; Mozos, J.-L.; Ordejon, P.; Taylor, J.; Stokbro, K. *Phys. Rev. B* **2002**, *65*, 165401.
- (38) Gronbeck, H.; Curioni, A.; Andreoni, W. *J. Am. Chem. Soc.* **2000**, *122*, 3839.
- (39) Hohenberg, P.; Kohn, W. *Phys. Rev.* **1964**, *136*, 864. Kohn, W.; Sham, L. J. *Phys. Rev.* **1965**, *140*, 1133. Ceperley, D. M.; Alder, B. J. *Phys. Rev. Lett.* **1980**, *45*, 566. Perdew, J. P.; Zunger, A. *Phys. Rev. B* **1981**, *23*, 5048.
- (40) Alavi, S.; Larade, B.; Taylor, J.; Guo, H.; Seideman, T. *Chem. Phys.* **2002**, *281*, 281.
- (41) Brédas, J. L.; Calbert, J. P.; da Silva Filho, D. A.; Cornil, J. *Proc. Natl. Acad. Sci. U.S.A.* **2002**, *99*, 5804.
- (42) (a) Engdahl, E.; Maniv, T.; Moiseyev, N. *J. Chem. Phys.* **1988**, *88*, 5864. (b) Galperin, M.; Beratan, D. N. *J. Phys. Chem. B* **2005**, *109*, 1473.
- (43) Büttiker, M.; Imry, Y.; Landauer, T.; Pinhas, S. *Phys. Rev. B* **1985**, *31*, 6207. Büttiker, M. *Phys. Rev. Lett.* **1986**, *57*, 1761; *IBM J. Res. Dev.* **1988**, *32*, 317; *Phys. Rev. B* **1988**, *38*, 9375.
- (44) For the monomolecule situation, we perform two separate calculations: one with the molecule covalently bonded on the left-hand side and one with it bonded on the right-hand side. The total current of the monomolecule case is the sum of the two, to guarantee the symmetric behavior on bias.